ELSEVIER

Enhanced photocatalytic degradation of methylene blue and methyl orange by ZnO:Eu nanoparticles

L. V. Trandafilović[*a], D. J. Jovanović[a], X. Zhang[b,c], S. Ptasińska[b,d], M. D. Dramićanin[a]

[a]*Laboratory for Radiation Chemistry and Physics, Vinča Institute of Nuclear Sciences, P.O. Box 522, 11001 Belgrade, University of Belgrade, Serbia*
[*]*lidija@vinca.rs*
[b]*Radiation Laboratory, University of Notre Dame,46556 Notre Dame, IN, USA*
[c]*Department of Chemistry and Biochemistry, University of Notre Dame,46556 Notre Dame, IN, USA*
[d]*Department of Physics, University of Notre Dame,46556 Notre Dame, IN, USA*

Abstract

ZnO nanoparticles doped with different Eu^{3+} percentages were synthesized in water (ZnO:Eu(x%)-W) and other solvents (methanol ZnO:Eu(x%)-M and ethanol ZnO:Eu(x%)-E). X-ray diffraction (XRD), transmission electron microscopy (TEM), X-ray photoelectron spectroscopy (XPS), optical absorption and photoluminescence (PL) spectroscopy were used for characterization of the nanoparticles. Our results showed influence of europium doping and solvents on size, particles agglomeration, light absorption and photocatalytic activity. Improvement in photocatalytical activity with addition of Eu^{3+} doping was detected. Particle size increased with Eu^{3+} doping in water samples, while it decreased in methanol. Agglomeration was more prominent in ZnO:Eu(x)-W samples.Greater amount of surface OH groups in case of ZnO:Eu(x%)-M samples was detected by PL, XPS and FTIR measurements. Influence of europium doping, as an electron trap, and surface OH groups, as a hole trap, was studied in sunlight photocatalytic degradation of cationic methylene blue (MB) and anionic methyl orange (MO). Improved photocatalytic behavior was discussed and influence of active species was further investigated using hole and hydroxyle radical scavengers. The degradation pathway of MB and MO, using high performance liquid chromatohraphy (HPLC), is also examined.

© 2016 Published by Elsevier Ltd.

Keywords: Zinc oxide, Doping, Europium, Surface OH, Photocatalysis, Methylene blue, Methyl orange

1. Introduction

Elimination of environmental pollution, by photocatalytic transformation of the organic pollutants into nontoxic molecules, becomes one of the widely researched topics [1–14]. Industrialization has led to considerably increase in a number of phenols, pesticides, dyes, solvents, and other organic pollutants with potentially carcinogenic intermediates in natural resources [15]. Aromatic azo-dyes, that cause hypersensitivity and allergies [16], are a major class of synthetic organic compounds and comprise about half of

the total world dye market released by many industries such as paper, plastic, leather, food, cosmetic and pharmaceutical [17, 18]. Various systems were used in photocatalytic degradation of dyes with different success, but semiconductors are among the most researched and employed in various formats: alone [19–23], defect-induced [24–26], doped [4, 5, 27–33], or combined with another material [10, 14, 34–36].

ZnO is a low cost semiconductor with wide bulk band gap (3.2 eV), large room temperature exciton (photoinduced electron-hole pairs) binding energy of 60 meV and excellent chemical and thermal stability [9, 37]. Due to its photosensitivity and catalytic properties it has been broadly studied as an efficient photocatalyst for the decomposition of many organic compounds [19, 20, 38]. However, ZnO photocatalytical efficiency is greatly hindered because of high recombination ratio of photoinduced electron-hole pairs, very poor response to visible light and high possibility of the photocorrosion.

In order to solve mentioned problems many researchers used doping (Al, Cu, Cd etc) or creating multi-component nanojunction system (Ag, Si, Au etc) on ZnO matrices [4, 10, 14, 27–29, 33–35]. For instance, doping with rare earth (RE) ions improved photocatalytic efficiency (through reducing the electron-hole pairs recombination), improved light absorption (through the creation of impurity energy levels within the band gap) while also advancing system PL emission (due their characteristic incompletely filled 4f shell) without blinking and photobleaching [28, 31, 32, 39–43]. Khatamian et al. [41] used La^{3+}, Nd^{3+} and Sm^{3+} doping to improve the photoactivity of ZnO in degradation of 4-nitrophenol. While Sin et al. [3, 44] greatly improved ZnO photochatalytical degradation efficiency of phenol under natural sunlight by doping ZnO with Eu^{3+} ions. The reports of Eu^{3+} doped ZnO nanoparticles in degradation of MO [45, 46] and MB [47] showed improved efficiency of doped samples under UV light.

Redox potential of the Eu^{3+} ion is -0.35 V (ZnO band gap is at -0.50 V versus NHE) [9, 31] so it can effectively trap the electrons from conducting band e^-_{cb} with partially filled f-orbital [32]. In similar manner, surface hydroxyl groups and methanol, can be used as hole traps [5, 48–51]. Surface OH groups and methoxide are formed during methanol reactions with oxygen on ZnO or TiO_2 nanoparticles surface [50–53]. This was main reason why we used methanol as a Zn ions solvent in our synthesis.

To the best of our knowledge this work reports for the first time on combined usage of surface OH groups (as a hole trap), and Eu^{3+} ions (as an electron trap), in ZnO:Eu nanoparticles for photocatalytical degradation of MB and MO. ZnO nanoparticles were synthesized with various doping percentages of Eu^{3+}, for which water (ZnO:Eu(x%)-W), methanol (ZnO:Eu(x%)-M) or ethanol (ZnO:Eu(x%)-E) were used. The synthesized nanoparticles were characterized by several techniques (UV-vis, PL, XRD, XPS, FTIR) and used for the photocatalytic degradation of cationic and anionic dyes, MB and MO, under simulated sunlight irradiation. MB and MO are commonly used materials in the dye industry and they are chosen because they are well-studied good representatives of acidic (anionic) and basic (cationic) dyes, offering better understanding of ionic interaction and its influence on photocatalytic degradation efficiency. The increased photoactivity of nanoparticles was discussed based on the separation process of electron-hole pairs and the

active species creation and detection.

2. Materials and methods

Materials used in our experiments are Zn-acetate (Zn(CH$_3$ COO)$_2$·H$_2$O, Sigma-Aldrich), sodium hydroxide (NaOH,Sigma-Aldrich), europium nitrate (Eu(NO$_3$)$_3$ ·H$_2$O, Sigma-Aldrich), methyl orange (C$_{14}$H$_{14}$N$_3$NaO$_3$S, Merck) and methylene blue (C$_{16}$H$_{18}$ClN$_3$S, Merck), acetonitrile (C$_2$H$_3$N), potassium iodide (KI), terephthalic acid (C$_8$H$_6$O$_4$, Sigma-Aldrich). All the reagents used in this work were of analytical grade without further purification.

2.1. Synthesis of ZnO and ZnO:Eu nanoparticles

The synthesis procedure of ZnO:Eu(x%)-W: 0.8 ml NaOH (1 M) was added into 2.45 ml of 4D aqueous solution, consisted of Zn-acetate (0.2 M) and europium nitrate (0.2 M). Zn^{2+} and Eu^{3+} ions were in corresponding ratios for 0, 1, 3, 5 and 10% Eu^{3+} doping.

The modified (non-water) synthesis of ZnO:Eu(x%)-M: ethanol solution of 0.8 ml NaOH (1 M) was added into 2.45 ml solution consisted of Zn-acetate (0.2 M) dissolved in methanol and europium nitrate (0.2 M) dissolved in ethanol (in ratios needed for 0, 1, 3, 5 and 10% Eu doping). In case of ZnO:Eu(x%)-E samples all salutes (Zn-acetate (0.2 M), NaOH (1 M) and europium nitrate (0.2 M)) were dissolved in ethanol. In both synthesis procedure, water and non-water solutions were treated in the same way, placed in a microwave oven and headed at 800 W for a period of time needed for reagents to react and samples to dry out (3 min 30 sec).

2.2. Characterization

X-ray diffraction measurements (XRD) were performed on a Rigaku Ultima IV diffractometer (CuK$_\alpha$ radiation λ = 0.154 nm). The transmission electron microscopy (TEM) measurements and electron diffraction (SAED) pattern were taken on JEOL JEM-2100 LaB 6. UV-vis absorption spectra of the nanoparticles were obtained by using a Perkin Elmer Lambda 5 UV-vis spectrophotometer. The photoluminescence (PL) spectra of the nanoparticles were recorded on a Perkin Elmer LS 3B spectrophotometer at the 320 nm excitation wavelength and Fluorolog-3 Model FL3-221 (Horiba Jobin-Yvon) was used for the 466 nm excitation.

FTIR spectroscopic analyses were carried out at room temperature using a Nicolet 380 spectrophotometer in the spectral range from 400 to 4000 cm^{-1}, with a resolution of 4 cm^{-1}. The datasets were averaged over 200 scans.

XPS measurement were done at a SPECS X-ray photoelectron spectrometer equipped with an X-ray tube, coupled to a Micro-FOCUS 600 X-ray monochromator, and a Phoibos 150 hemispherical energy analyser attached to an analysis chamber. The base pressure in the analysis chamber was kept below 1×10^{-9} mbar. The monochromatized aluminum (Al) K$_\alpha$ (1486.6 eV) X-ray beam was produced at a power of 100

W with an anode voltage of 15 kV and a current of 6.7 mA. The full width at half maximum (FWHM) of the Au $4f_{7/2}$ peak for 20 eV pass energies was 0.5 eV. The survey spectrum was recorded using an energy step of 1 eV and a pass energy of 70 eV. High resolution photoelectron spectra were obtained using an energy step of 0.05 eV and a pass energy of 20 eV. A flood gun with 1 eV electron beam (10 μA emission current) was used to neutralize possible surface charging. The binding energy (BE) of the C 1s peak at 284 eV was used for the BE calibration.

High performance liquid chromatohraphy (HPLC) analyses were performed using a Waters 600E chromatograph with a reversed-phase column (Jupiter C18, 5 μm, 250 x 4.6 mm) at 40 °C. For MO degraded samples gradient composed of solution A (10.0 mM ammonium acetate solution) and solvent B (acetonitrile) was used. The gradient conditions were as follows: 0-5 min, hold at 2.5% B; 5-10 min, a linear increase from 2.5 to 5% B; 10-15 min, a linear increase from 5 to 99% B; 15-35 min, hold at 99% B. The flow was set at 0.2 ml/min. In case of MB solution, a mobile phase acetonitrile-ammonium acetate had 40/60 (v/v) ratio with flow 0.2 ml/min. Waters UV detector was set at 465 nm (for MO) and 664 nm for MB. 2 μl of sample was injected by using autosampling device. The eluents from the chromatographic column successively entered the UV-Vis detector.

The zeta potential measurements on 0.02 ppm concentrated samples without any further treatmen were performed by ZetaPALS instrument.

An average hydrodynamic diameter was recorded at Brookhaven Instruments light scattering setup BI-200SM with goniometer 80-1600 and correlator BI-9000AT, using argon ion laser operating at 514 nm. The temperature was equilibrated to 25 °C, and the pH was varied in the 6-10 range using 0.001M $HClO_4$ or 0.15M NaOH prior to collecting the data. The effect of pH on average hydrodynamic diameter was studied for ZnO:Eu materials by optical method (dynamic light scattering).

2.3. Photocatalytic activity

For study of photocatalytic activity, 1 mg per 1.0 mL of the ZnO or ZnO:Eu samples with various Eu^{3+} loadings were dispersed in 10 ppm aqueous solution of methylene blue or methyl orange. After sonication for 60 min in the dark, needed for absorption-desorption equilibrium to be achieved, the solutions were placed in a quartz cell and irradiated by using an Osram Vitalux lamp at 300 W. The emission spectrum of the lamp simulates solar radiation. The lamp was located at the distance of 50 cm above the top surface of the dye solution. Absorption spectra of the solution were recorded at certain time intervals.

2.4. Detection of active species

The formation of •OH radicals by the photoirradiated ZnO and ZnO:Eu samples was detected by photoluminescence (PL) technique with terephthalic acid (TA) as the probe molecule. Due to reaction with •OH radicals TA produces highly fluorescent product, 2-hydroxyterephthalic acid (HTA), which shows the

PL signal at 425 nm. In experimental procedures nanoparticles were added to the 1×10^3 M TA aqueous solution with a concentration of 2×10^3 M NaOH. PL spectra of generated HTA were then recorded on a Perkin Elmer LS 3B spectrophotometer at a 280 nm excitation after 15 min of irradiation. In order to investigate the dominant influence of active species on dye degradation, hydroxyl and hole scavengers were used. Acetonitrile was used as hydroxyl radical scavenger allowing us to research consequence of hole on dye degradation. In the same maner potassium iodide (KI) was used as a hole scavenger. Dye (MB or MO), in concentration of 10 ppm, was dissolved in acetonitrile (hydroxyl radical scavenger), prior to the sample adding and lamp irradiation. Elimination of hole was done through dissolving potassium iodide in solution of interest.

2.5. Total organic carbon determination

The total organic carbon (TOC) was determined by using Lab-TOC Model 2100. Equal amounts (25 mg) of ZnO:Eu(1%)-W photocatalyst were added into two glasses that contained 25 ml of the 50 ppm MO solution. Same was done with ZnO:Eu(3%)-W in MO and with ZnO:Eu(1%)-M and ZnO:Eu(10%)-M in MB solution. The choice of the samples were dictated by their success in dye degradation. After mixing for 60 min in the dark the first glass with solution was kept in the dark at room temperature, while the second was irradiated with an Osram Vitalux lamp for 90 min. After irradiation both samples were centrifuged for 15 min with 4000 rpm in order to remove the photocatalyst from the solution and the TOC was determined in remaining solution by equation reported elsewhere [54].

3. Result and discussion

3.1. Morphology and structure

XRD spectra of ZnO:Eu(x%)-M (x= 0%, 1% and 3% Eu doping) samples compared to ZnO hexagonal bulk (ICSD #29272) are presented in Figure 1. The peaks are identified as (1 0 0), (0 0 2), (1 0 1), (1 0 2), (1 1 0) and (1 0 3) planes of the hexagonal zinc oxide structure [55]. No europium oxide or impurity phases were detected. However, the shift of the (002) peak position, as a function of Eu^{3+} ion doping percentage, is observed (inset of Figure 1). The shift correlates with distortion of the ZnO crystal structure due to the difference of Eu^{3+} and Zn^{2+} ionic radius [56].

Figure 2 (a and b) shows TEM images of the ZnO:Eu(1%)-W and ZnO:Eu(1%)-M samples. Magnified crystal structure and ring electron diffraction patterns are displayed at upper and lower insets. The differences in particle size, shape, and distribution are detected for different solvents used in synhesis. From particle size distribution (not presented here) of ZnO:Eu(1%)-W we calculated average size around 16.2 nm and a broad size distribution (FWHM=8.86 nm). The distance between the two adjacent planes, estimated from the lattice fringes (inset Figure 2a), is found to be 0.52 nm corresponding to (001) plane spacing [57].
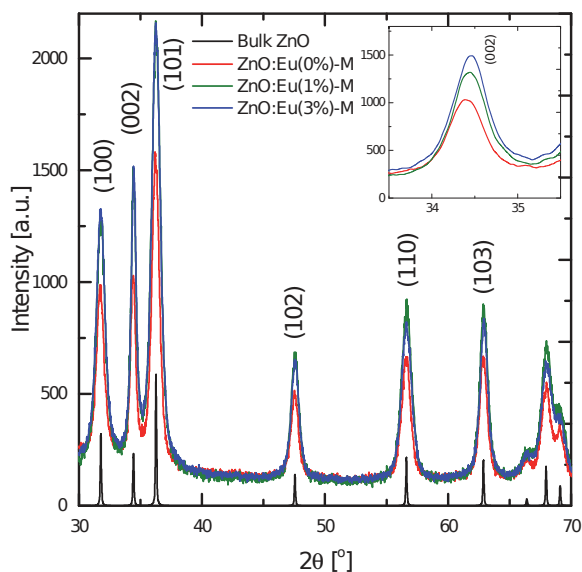
Fig. 1. XRD patterns of pure ZnO and ZnO:Eu(x%)-M nanostrucutures with different doping contents of Eu^{3+} (x=1% and 3%). Inset is the magnified region of (0 0 2) peak.

In the case of the ZnO:Eu(1%)-M we detected spherical nanoparticles, with an average diameter of 5.6 nm (particle size distribution not presented here) and a narrow size distribution (FWHM=2.62nm). The distance between the adjacent lattice fringes is 0.28 nm, which reveals the (100) planes (inset Figure 2b). In both cases, the ring electron diffraction patterns indicates a hexagonal crystal structure of ZnO.
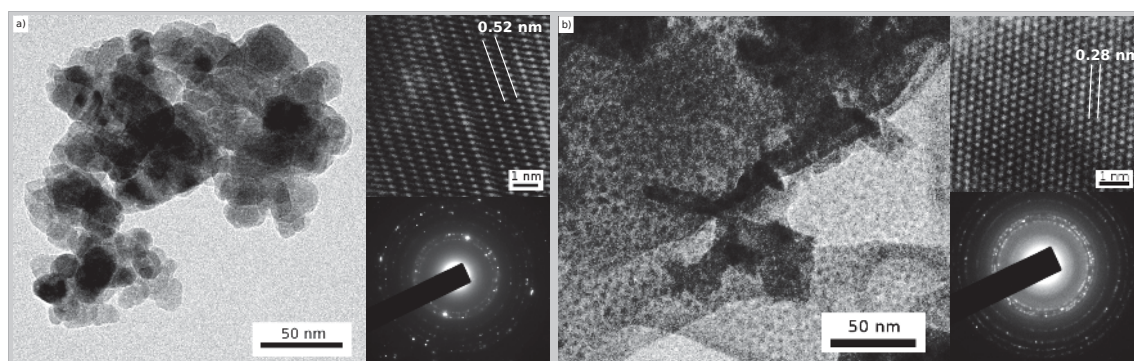

Fig. 2. TEM images of (a) ZnO:Eu(1%)-W and (b) ZnO:Eu(1%)-M nanoparticles. Crystal planes and obtained electron diffraction (SAED) patterns are presented in upper and lower insets for both samples.

3.2. Spectroscopic studies

The absorption spectra of europium doped ZnO samples, for water and methanol, are presented in Figure 3. We detected blue shifts of all absorption band edges compared to ZnO bulk value (380 nm) due to the quantum confinement, indicating the presence of nano-size particles. The influence of solvents on peak shifts

and shapes was also observed. As seen in Figure 3a, with larger percentage of Eu^{3+} doping peaks are shifted from 361 nm (x=0% pure ZnO) to 371 nm (x=5%), implying growth or agglomeration of nanoparticles. On the other hand, in Figure 3b, the shift from 362 nm (x=0%) to 353 nm (x=10%) implied reduced particle size in the case of ZnO:Eu(x%)-M samples. These findings are in consistency with TEM measurements presented in Figure 2.
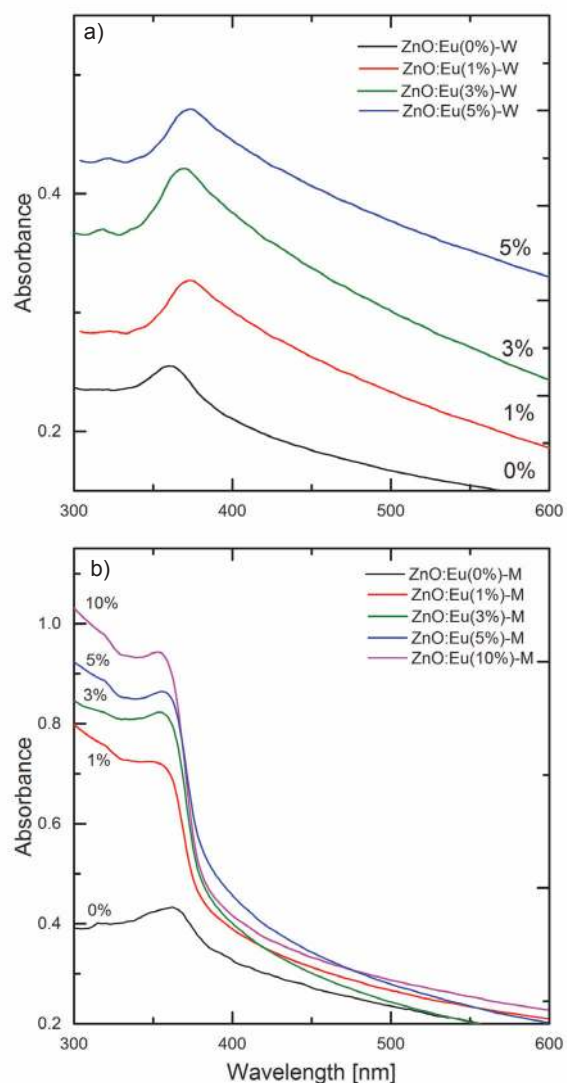

Fig. 3. Absorption spectra of a) (ZnO:Eu(x%)-W and b) (ZnO:Eu(x%)-M nanoparticles solutions for doping contents x% of Eu^{3+}

Photoluminescence spectra are presented in Figure 4 showing the results under two different excitation at 320 nm (which is not absorbed by Eu^{3+} ions) and 466 nm (which is absorbed by Eu^{3+} ions) for ZnO:Eu(x%)-W and ZnO:Eu(x%)-M samples. Under excitation at 320 nm all samples show band to band emission. Depending on a Eu^{3+} percentages, for ZnO:Eu(x%)-W, band to band emission are in range from 385 nm to

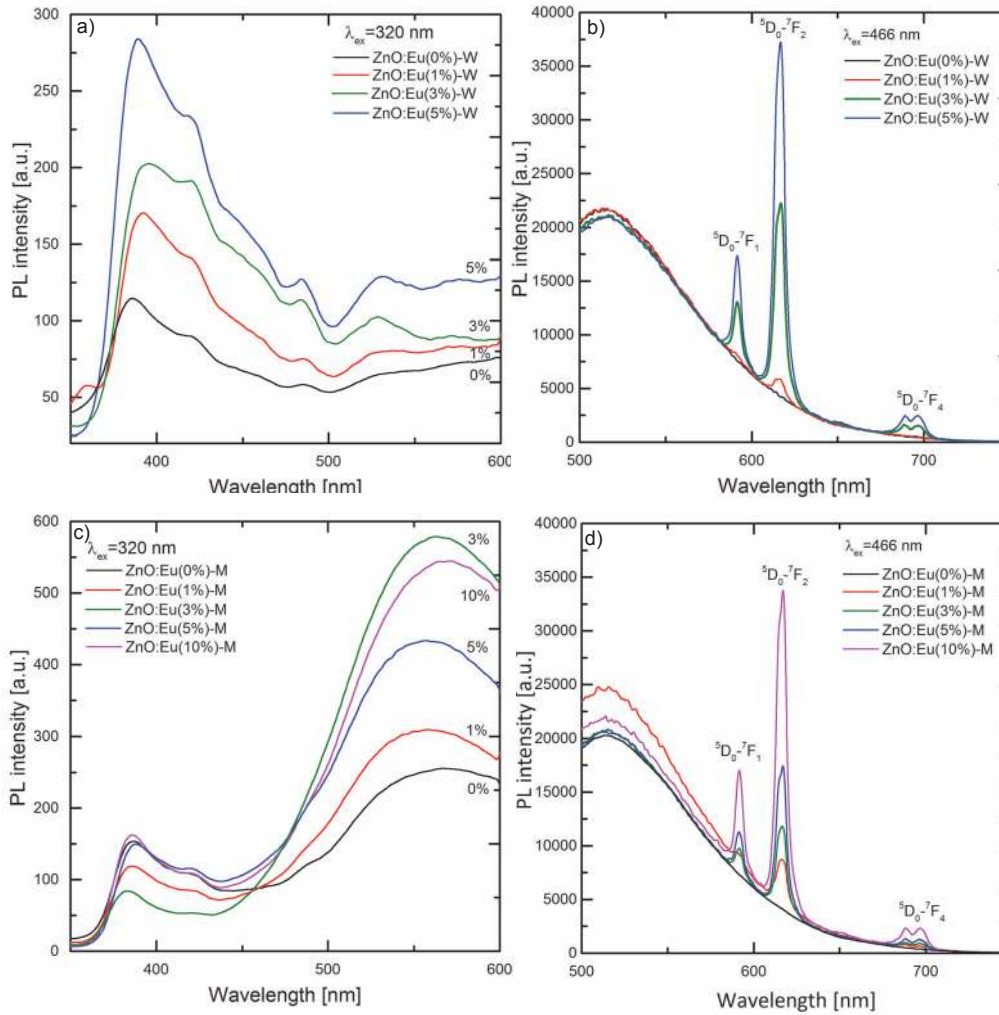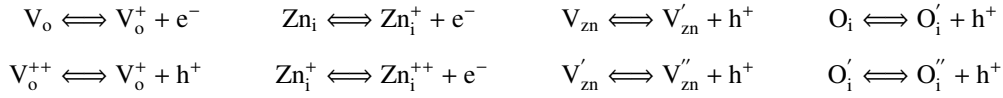389 nm, while for ZnO:Eu(x%)-M in 381-386 nm range.

Fig. 4. Room temperature PL emission of a) ZnO:Eu(x%)-W with excitation wavelength λ_{ex}=320 nm b) ZnO:Eu(x%)-W, λ_{ex}=466 nm, c) ZnO:Eu(x%)-M λ_{ex}=320 nm; d) ZnO:Eu(x%)-M λ_{ex}=466 nm

There are six kinds of defects in ZnO crystal structure that contribute to the emission at wavelengths higher than 400 nm. Oxygen vacancies (V_o) and zinc vacancies (V_{zn}), coming from the Schottky reaction (equation 1a), zinc interstitials (Zn_i) arise from Frenkel reaction (equation 1b), oxygen interstitials (O_i) appear in the system rich with O_2 (equation 1c) [58, 59]. Oxygen antisites (Zn_O), and zinc antisites (O_{Zn}) are also contributor to rich defect emission of ZnO.

$$0 \Longleftrightarrow V_{zn} + V_o \tag{1a}$$

$$Zn_{zn} \Longleftrightarrow Zn_i + V_{zn} \tag{1b}$$

$$\frac{1}{2}O_2 \Longrightarrow O_i \tag{1c}$$
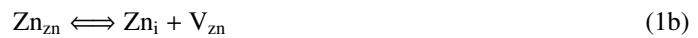
Further ionization of V_o, Zn_i, V_{zn} and O_i leads to:

$$V_o \Longleftrightarrow V_o^+ + e^- \qquad Zn_i \Longleftrightarrow Zn_i^+ + e^- \qquad V_{zn} \Longleftrightarrow V_{zn}' + h^+ \qquad O_i \Longleftrightarrow O_i' + h^+$$

$$V_o^{++} \Longleftrightarrow V_o^+ + h^+ \qquad Zn_i^+ \Longleftrightarrow Zn_i^{++} + e^- \qquad V_{zn}' \Longleftrightarrow V_{zn}'' + h^+ \qquad O_i' \Longleftrightarrow O_i'' + h^+$$

Although different transition can result in similar emission, main contributions to the rich ZnO luminescence are coming from oxygen vacancies and zinc interstitials. For instance, peak at 421 nm is due to carrier recombination between zinc interstitial (Z_{ni}) and hole in the valance band, while the emission at 485 nm comes from the single ionized oxygen vacancies (V_o^+) or/and charged zinc vacancy (V_{zn}') [58–62]. The PL spectra in green and yellow region show main difference between ZnO:Eu(x%)-W and ZnO:Eu(x%)-M samples. After using methanol, we detected a strong and broad band around 550 nm. Green emission is the result of the existence of singly ionised oxygen vacancy (V_o^+) while some researchers attributed green and yellow emission to the surface OH or $Zn(OH)_2$ groups [63, 64]. Which in this case coincides with methanol degradation to surface OH and methoxide at the ZnO surface [52]. Dominant emission from Eu^{3+} f-f transitions are detected after excitation at 466 nm (Figures 4b and 4d). Lines at 591, 619 and 701 nm correspond to europium characteristic $^5D_0 \rightarrow \, ^7F_1$, $^5D_0 \rightarrow \, ^7F_2$ and $^5D_0 \rightarrow \, ^7F_4$ transition, respectively [65–67]. The emission intensity has increased with increasing of Eu^{3+} ion concentration, but in case of ZnO:Eu(x%)-M samples intensity is smaller when compared to ZnO:Eu(x%)-W samples.
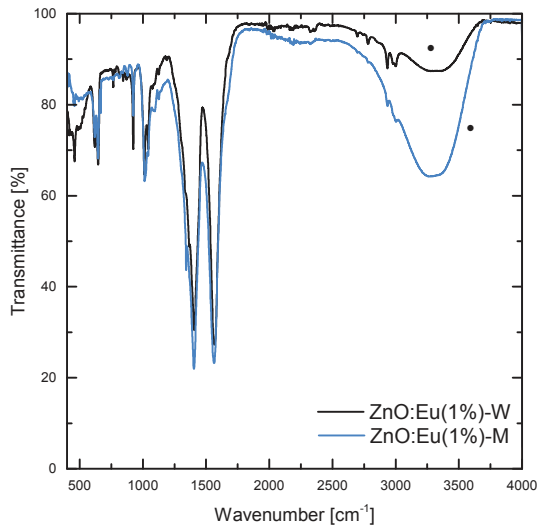

Fig. 5. FTIR spectra of ZnO:Eu(1%)-W and ZnO:Eu(1%)-M samples.

In Figure 5 the FTIR spectra of ZnO:Eu(1%)-W and ZnO:Eu(1%)-M samples are presented. Zinc oxide absorption band with stretching mode of Zn-O was detected at 458 cm^{-1} [68, 69]. The absorption bands at 1343 cm^{-1}, 1448 and 1563 cm^{-1} were assigned to the symmetric and asymmetric stretching vibration of

the carboxylate group from the acetate anion. New line detected in ZnO:Eu(1%)-M sample at 1350 cm^{-1} is assigned to CH_3 vibration due to methanol used in synthesis [68]. OH ion presence can be confirmed by the strong stretching mode at about 3247 cm^{-1} and a corresponding bending mode at about 1600 cm^{-1} present only in ZnO:Eu(1%)-M sample [70]. However, it should be taken into account that presence of these modes could also be due to presence of water adsorbed on the surface of the samples or in the environment around the samples [71, 68].

3.3. XPS

The chemical composition of ZnO:Eu(5%)-W and ZnO:Eu(5%)-M, studied by XPS analysis, is presented in Figure 6. The XPS survey spectrum (not shown here) indicates peaks of Zn, O, C, Au and Na. Detected gold came from the substrate and is used for binding energy calibration. After peak decomposition of the high-resolution O 1s region (Figure 6a), there are two contributions in a case of ZnO:Eu(5%)-W (531.0 and 531.7 eV) and three contributions (530.3, 531.7 eV and 532.0 eV) in case of ZnO:Eu(5%)-M sample. The component at 530.3 eV is attributed to the O^{2-} ions in Zn-O-Zn [52], the components at 531.7 and 532.0 eV belong to surface OH groups [20, 29]. A higher energy peak at 532.0 eV can also be attributed to the methanol adsorption at a ZnO surface [52]. The analysis of the Zn 2p photoelectron spectra revealed presence of Zn $2p_{3/2}$ and Zn $2p_{1/2}$ peaks located at 1022.0 eV and 1045.0 eV, respectively [72]. The peak at 1022.0 eV is characteristic of Zn^{2+} ion in an oxide environment [39]. The C 1s XPS spectra presents two peaks (285.5 eV and 289 eV) that exist in both ZnO:Eu(x%)-W and ZnO:Eu(x%)-M samples, while the peak at 284.2 eV is present only in the ZnO:Eu(x%)-M sample. The peaks at 285.5 eV and 289.0 eV are assigned to C-O bond and acetate species, respectively [73, 74]. The peak at 284.2 eV belongs to the surface CH_3 from the methoxy group (-OCH_3) and adsorbed methanol [52, 75, 76]. The Eu 3d XPS spectra of ZnO:Eu(5%)-W and ZnO:Eu(5%)-M samples are presented in Figure 6d. Both spectra have four peaks coming from the multiple spin-orbit interactions (J = 3/2 and 5/2 components of Eu 3d). The peaks at 1135.0 and 1164.6 eV belong to Eu^{3+} $3d_{5/2}$ and $3d_{3/2}$ respectively, while 1125 eV and 1155 eV are from Eu^{2+} $3d_{5/2}$ and $3d_{3/2}$ energy levels [27, 73, 77]. The energy difference between the two Eu^{3+} lines, j-j energy separation, is 29.4 eV and is in good agreement with literature values for oxygen-coordinated europium ions [77]. In general, the peak intensities for the ZnO:Eu(5%)-M sample are much smaller than ZnO:Eu(5%)-W sample, implying the lower amount of Eu ions that are incorporated into ZnO crystal structure and/or that Eu ion peaks are partially screened by the surface methanol and methoxy group, detected in C 1s XPS spectra [78, 77].

3.4. Photocatalytical activity

The results of the photocatalytic activities of ZnO nanoparticles (with and without Eu^{3+} ions), evaluated by the photodegradation of methylene blue and methyl orange, are presented in Figure 7. In subfigures
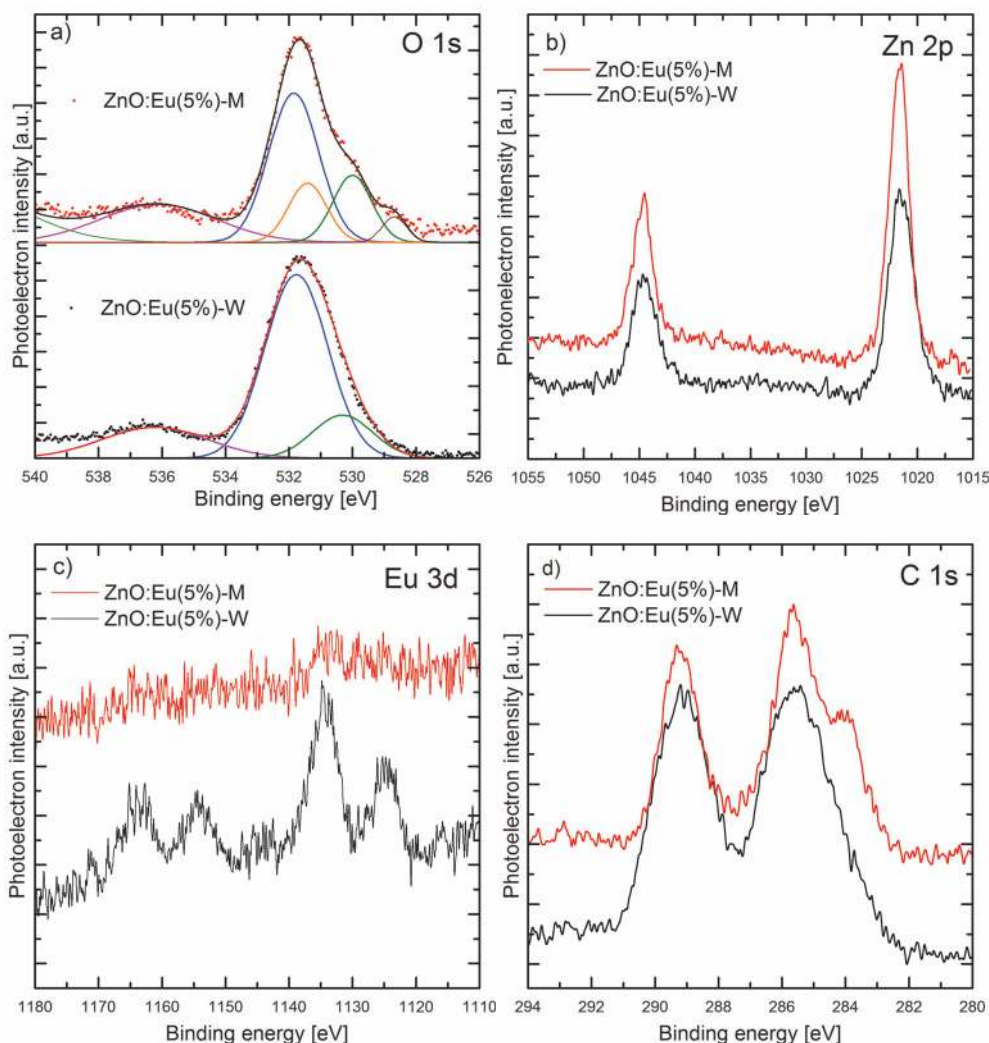
Fig. 6. XPS spectra of ZnO:Eu(5%)-W and ZnO:Eu(5%)-M a) O1s peaks; b) Zn 2p peaks; b) Eu 3d peaks and c) C 1s peaks.

7a and 7b are the results for ZnO:Eu(x%)-W for MB and MO while at 7c and 7d are ZnO:Eu(x%)-M results for the same dyes. Pure ZnO shows the lowest photocatalytical activity due to the fast recombination of photogenerated electrons and holes [2]. In order to inhibit e-h recombination Eu^{3+} ion was used as an effective electron trap through importing new energetically favorable levels [4, 9, 33]. As presented, doped systems demonstrate higher photocatalytical activity (Figure 7a and 7b). The best performance was exhibited for ZnO:Eu(1%)-W with degrading MB to 10% after 150 min, while ZnO:Eu(3%)-W was most effective in MO degradation, showing 62% of dye degradation within 150 min. In similar manner as Eu^{3+} which acted as a electron trap, surface hydroxyl groups, after irradiation, act as a hole trap, adsorption sites and sources of the •OH radicals [5, 48, 49]. Accordingly, the photocatalytic activity will increase with the

increase of the hydroxyl groups on the catalyst surface, giving the rationale for raising their number. When methanol is used as a solvent in the synthesis, results from PL spectra (Figure 4c) and XPS spectra of the O 1s region (Figure 6c) imply an increase in the amount of OH groups. As expected, methanol modified samples show rise in photocatalytical degradation of methylene blue and methyl orange. The plot of dye concentration (MB and MO) as a function of irradiation time in a presence of the ZnO:Eu(x%)-M samples is presented in Figure 7c and 7d, respectively. For MB, best performance was detected for 1% Eu^{3+} doping. Although the dye concentration after 150 min of irradiation is 10%, as in a case of ZnO:Eu(1%)-W sample, the ZnO:Eu(1%)-M was more efficient in first 60 min. Interestingly, the best result for MO photodegradation is for the sample with 10% Eu doping (ZnO:Eu(10%)-M), complete colour degradation was observed after 60 min (Figure 7d).

The results of modified samples were better than Degussa (P25), which degraded MB to 35% and MO to 40% after 60 min of irradiation (Figure 7c and d). Blank experiments performed without any catalysts or without illumination but in the presence of catalyst (Figure 7), show that there is small degradation of dyes in the dark in the presence of catalyst (2% for MO and 3% for MB after 60 min) and small degradation of dyes without catalyst under light (6% for MO and 11% for MB after 150 min), indicating that the catalyst and light are essential for the fast photocatalytic degradation.

Ionic configuration and structures of the dyes (MB is cationic dye while MO is anionic) are the main reasons for differences between the result in photodegradation of the dyes. For instance, dye degradation by $^{\bullet}$OH radicals can happen near the surface of modified nanoparticles, since $^{\bullet}$OH radicals have short life time. MB as a cationic dye, with $C-S^+=C$ functional group (Figure 12a), will interact through Columbic forces with anionic elements of ZnO:Eu system (O^{2-}, OH^-) [1]. On the other hand, as anionic dye, MO with a reactive SO_3^- group (Figure 10c) will react with cationic elements (Zn^{2+}, Eu^{3+}). The results presented in Figure 7, imply that using methanol as the solvent greatly improves the number of anionic elements on ZnO:Eu surface, thus enhancing degradation of MB. With a greater amount of Eu^{3+} ion loading (i.e. 10%) the system becomes more efficient in degrading MO. This also allows the use of modified ZnO:Eu for selective pollutant degradation. For instance ZnO:Eu(1%)-M effectively degraded MB, while MO degradation was weak. On the other hand, ZnO:Eu(10%)-M was weak in degrading MB while completely decolorized MO in 60 min. According to Ramesha et al. [79] and Lazar et al. [80], a surface charge is the essential parameter for selective removal of pollutants. Taking into account all that is said, the effect of pH on a photocatalytical efficiency can be expected. The reported isoelectric point (PZC) for ZnO varies between pH 8.7-10.3 [81]. This means that pH values higher than ZnO isoelectric point are favorable for the adsorption of positively charged dye (MB), while for pH values lower than the PZC, adsorption of negatively charged dye (MO) are preferred. When we changed the pH values of a system containing ZnO:Eu(1%)-W sample and MB dye toward a higher values (pH=12), slight improvement in photodegradation of MB is detected. Conversely, the reduction of a pH (pH=6) resulted in decrease of photocatalytic degradation of MB. When
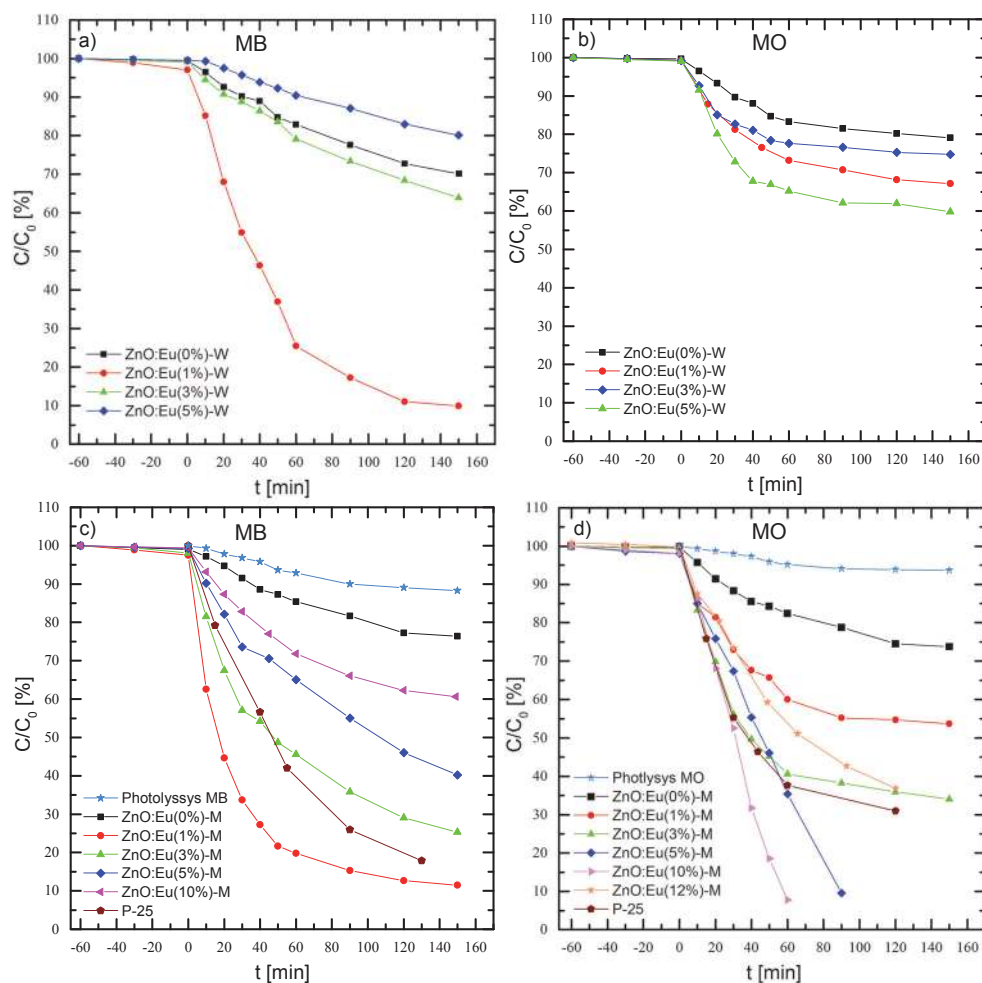
Fig. 7. Effect of Eu^{3+} doping content in ZnO:Eu(x%)-W on a) MB b) MO; and in ZnO:Eu(x%)-M on c) MB d) MO concentration. Dyes concentration are 10 ppm, photocatalyst amount is 1 mg per 1 ml of dye.

the efficiency of MO degradation as a function of pH values are tested in a presence of ZnO:Eu(3%)-W sample, the most effective degradation was at pH value of 7. It should be noted that for lower pH values ZnO particles dissolution hinder photocatalytical efficiency [82].

Isoelectric point (ISP) was measured for the most effective samples by zeta potential in a function of pH (Figure C4 Supplemental material). The measured isoelectric point was then compared with ISP results achieved by measuring agglomeration of nanoparticles solution as a function of pH (Figure C5 Supplemental material) [83]. Isoelectric points from zeta potential for samples ZnO:Eu(1%)-W, ZnO:Eu(1%)-M and ZnO:Eu(10%)-M are as follow: 8.31, 7.32 and 8.35. On the other hand, ISP result from agglomeration technique for ZnO:Eu(x%)-W are 8.2, 8.4, 8.75 for 0%, 1% and 5%. For ZnO:Eu(1%)-W sample agglomeration technique have good agreement with zeta potential measurement while for methanol samples agglomeration

technique overestimated ISP point probably due to complex surface of nanoparticles. The ISP results from agglomeration technique for ZnO:Eu(x%)-M systems are 7.5, 7.74, 8 and 8.5 for 0%, 1%, 5% and 10% of Eu^{3+} doping, respectively. However, it can be noticed that with Eu^{3+} doping ISP is shifted toward higher values and that samples synthesized in methanol have lower ISP than samples synthesized in water. Results for ISP allow better understanding of samples MO and MB photocatalytical degradation efficiency. For instance, mixture of MO and ZnO:Eu(1%)-W sample has pH=9.1 which is higher than pH of nanoparticles ISP (8.31), meaning that the negatively charged nanoparticles interact with anionic MO (pH of a system is above nanoparticles ISP) and photocatalytical activity is low, as recorded in Figure 7b. ZnO:Eu(1%)-M sample ISP point is 7.32, while MO and the sample solution has a pH=7.7, which again means negatively charged particles and anionic dye giving low photocatalytical efficiency. But, as mentioned earlier, doping with Eu^{3+} ions shifts nanoparticles ISP toward higher values, and as recorded (Figure 7d), gives better results for photodegradation of MO. For ZnO:Eu(10%)-M sample, ISP is shifted above pH of solution resulting in better dye degradation. MB and ZnO:Eu(1%)-W solution had pH=10.1 which is above nanoparticles ISP (8.31) giving good photocatalytical degradation. The same is for ZnO:Eu(1%)-M and MB solution where pH is 7.9, which is again above nanoparticles ISP (7.32).

Methanol as a source of a ZnO:Eu(x%)-M samples surface modification [50–53], were tested through elimination of methanol from synthesis. The Eu^{3+} doped ZnO samples where all solutes were dissolved in ethanol (methanol was excluded) were denoted as ZnO:Eu(x%)-E samples. Results for MB and MO dye degradation, presented at supplementary material (Figure A.1.), show that the best result in MB and MO degradation is for the ZnO:Eu(3%)-E sample, with colour degradation to 45% and 50% after 150 min for MB and MO respectively. With removal of methanol from synthesis, samples efficiency in photocatalytic dye degradation become weaker compared to ZnO:Eu(x%)-M samples.

The dye degradation process induces both decoloration (breaking of the dye molecule) and degradation of its aromatic structure. The efficiency of dye mineralization was quantify on most effective samples in MO (ZnO:Eu(10%)-M, ZnO:Eu(3%)-W) and MB degradation (ZnO:Eu(1%)-M and ZnO:Eu(1%)-W), by the percentage removal of total organic carbon. After 90 min irradiation, the photochemical mineralization of methyl orange for ZnO:Eu(10%)-M and ZnO:Eu(3%)-W was 45.4% and 15%, respectively. For methylene blue, TOC for ZnO:Eu(1%)-M and ZnO:Eu(1%)-W, samples was 33.6% and 25.4%. Results imply that the chemical interactions between dye - active sites with the photocatalyst are important and are governed by the composition and polarity of the dye groups linked to the surface.

3.5. Kinetics rate

In order to examine the controlling mechanism of the adsorption process, a pseudo-first order kinetics (according to the Langmuir-Hinshelwood model) (FO) [2, 13, 84] and pseudo second-order equation (SO)
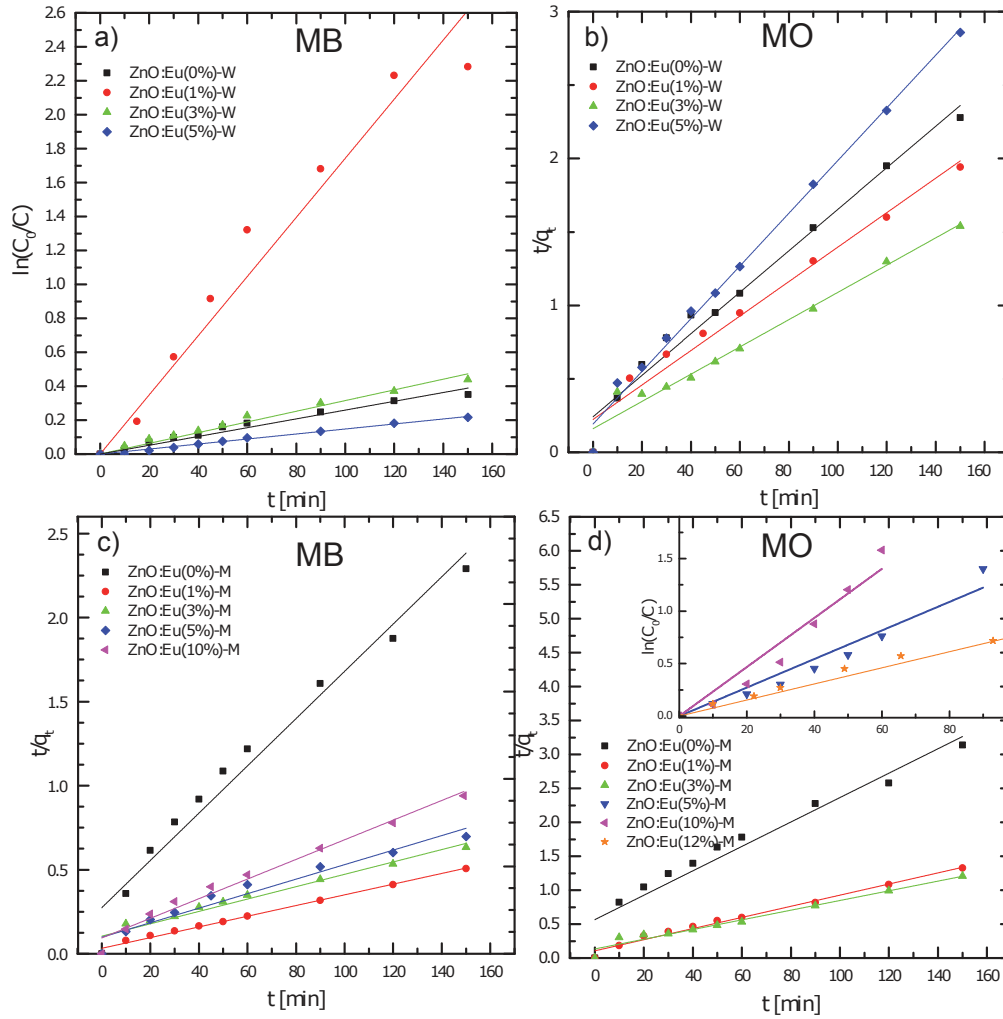
Fig. 8. Pseudo-first-order linear plots of $\ln(C_o/C)$ (figure a and inset in figure d) and pseudo-second-order linear plots of t/q_t (figures b,c and d) versus irradiation time for the degradation kinetics of MB and MO using different photocatalysts.

[85, 86] were used,

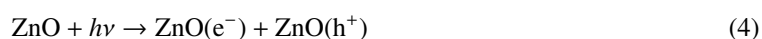$$ln(C_0/C) = k_{abs}t \tag{2}$$

$$t/q_t = 1/k_2 q_e^2 + t/q_e \tag{3}$$

where k_{abs} is FO [min^{-1}] and k_2 is pseudo SO [g·mg^{-1}·min^{-1}] rate constant of adsorption. The adsorption capacity at the time t and at the equilibrium is q_t and q_e [mg·g^{-1}], respectively. The equations details are given in supplementary material (Supplementary B). Plots of $\ln(C_0/C)$ and t/q_e versus t, are presented in Figure 8.

As expected, kinetics depend on the ionic configuration of the dye and reactive surface of nanoparticles. In the case of ZnO:Eu(x%)-W degradation of MB follow pseudo first order while with MO pseudo second-

order. The pseudo second-order kinetics suggest that the adsorption process may have character of chemical sorption involving valence forces through sharing or exchanging of electrons between adsorbent and sorbate [85–88]. When methanol was used as the solvent, picture is partially reversed, photodegradation of MB now follows pseudo SO kinetics, while photocatalysis of MO follow the pseudo SO for lower Eu^{3+} percentage and pseudo FO for $\geq$ 5% of Eu^{3+} doping. In case of MO strong photocatalytical efficiency of 10% Eu^{3+} doped system is probably due to the superposition of multiple factors like a positive charge of Eu^{3+} ions, better surface charge separation etc. Although this will be mentioned in the next subsection, a more detailed picture of processes will be thematic of our next paper.
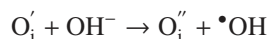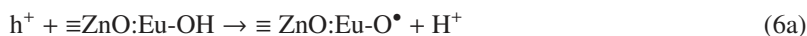
3.6. Detection of active species and possible degradation mechanism

In order to investigate photocatalytic mechanisms influence of different active species scavenger (acetonitrile, potassium iodide, terephtalic acid) on the degradation of MB and MO were studied. When a semiconductor is irradiated with photon that has energy equal or larger than semiconductor band gap, electron-hole pair (exciton) is created. The electron is excited to conductive band and the hole is created in the valence band. After charges are separated the electron can diffuse toward the surface, with or without recombination hole. As mentioned above, fast recombination of exciton can drastically decrease photocatalytical efficiency. With Eu^{3+} doping, the electron is trapped to the energetically favorable Eu^{3+} ion (equation 5a) and is inhibited to recombine with hole [32] creating super oxide radicals ($O_2^{\bullet-}$) (equation 5a), as presented at energy level scheme (Figure 9). An electron can be transferred to ionised oxygen vacancies V_o^{++}, (equation 5b) [89] leading to reaction with adsorbate O_2 creating super oxide radicals ($O_2^{\bullet-}$). When Eu^{3+} ions are introduced to ZnO structure higher amount of produced $O_2^{\bullet-}$ radicals lead to the stronger photocatalyitic activity. Electron can react with adsorbed H_2O [3, 7, 9, 11, 58].

$$ZnO + h\nu \rightarrow ZnO(e^-) + ZnO(h^+) \tag{4}$$

$$e^- + Eu^{3+} \rightarrow Eu^{2+}$$
$$Eu^{2+} + O_2 \rightarrow Eu^{3+} + O_2^{\bullet-} \tag{5a}$$

$$e^- + V_o^{++} \rightarrow V_o^+$$
$$V_o^+ + O_2 \rightarrow O_2^{\bullet-} \tag{5b}$$

$$e^- + O_2^{\bullet-} + 2H^+ \rightarrow H_2O_2$$
$$e^- + H_2O_2 \rightarrow OH^- + {}^\bullet OH \tag{5c}$$

At the same time, photogenerated hole in the valence band is trapped by surface hydroxyl group (equation 6a), reacts with ionised oxygen interstitial (equation 6b) [89, 58] or reacts with adsorbed water (equation

6c), by interfacial charge transfer, creating highly reactive hydroxyl radical ($^\bullet$OH) [11, 58].

$$h^+ + \equiv ZnO{:}Eu\text{-}OH \rightarrow \equiv ZnO{:}Eu\text{-}O^\bullet + H^+ \tag{6a}$$

$$O_i'' + h^+ \rightarrow O_i' \tag{6b}$$

$$O_i' + OH^- \rightarrow O_i'' + {}^\bullet OH$$

$$h^+ + (H_2O \rightarrow H^+ + OH^-) \rightarrow H^+ + {}^\bullet OH \tag{6c}$$

In the process of degradation, dyes are first oxidized through the successive attack of hydroxyl radical $^\bullet$OH [1] and/or through hole transfer (equation 7a). After oxidation, intermediates are self degraded or they are degraded by reactive oxidative species (ROS) to final products [90]:
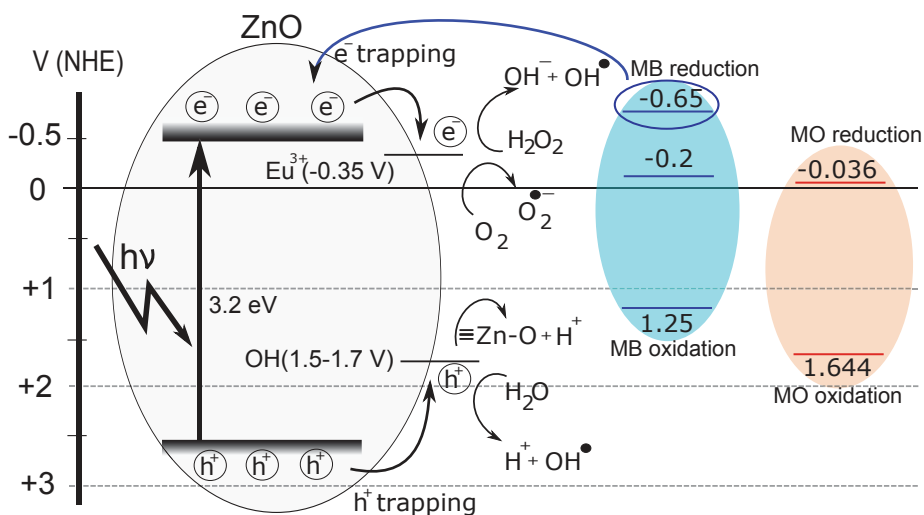
$$Dye + ({}^\bullet OH \text{ or } h^+) \rightarrow Dye^{\bullet +} \tag{7a}$$

$$Dye^{\bullet +} \rightarrow Intermediates + ROS \rightarrow Degradation\ products. \tag{7b}$$

Fig. 9. Scheme of the energy levels in Eu^{3+} doped ZnO with possible photocatalytic mechanism of MB and MO degradation.

In the case of MB, oxidation process can be caused by electron injection into ZnO nanoparticles but only with the singlet excited state of MB [91], as presented in Figure 9. A vast number of researchers consider hydroxyl radicals to be the most important active species in pollutant degradation [3, 24]. To test hydroxyl radical production from our samples photoluminescence of terephtalic acid was used. The TA-PL emission spectra of different ZnO:Eu samples excited at 280 nm were measured after 15 min irradiation. The result presented in Figure 10, shows the existence of the PL peak at about 425 nm arising from the hydroxylation of terephthalic acid. Because the intensity of the PL peak of 2-hydroxyterephtalic acid is in proportion to the amount of produced $^\bullet$OH radicals we can conclude that ZnO:Eu(1% and 5%)-M (Figure 10a) produce more $^\bullet$OH radicals when compare to the ZnO:Eu(1% and 3%)-W samples. TA-PL spectra of ZnO:Eu(1%
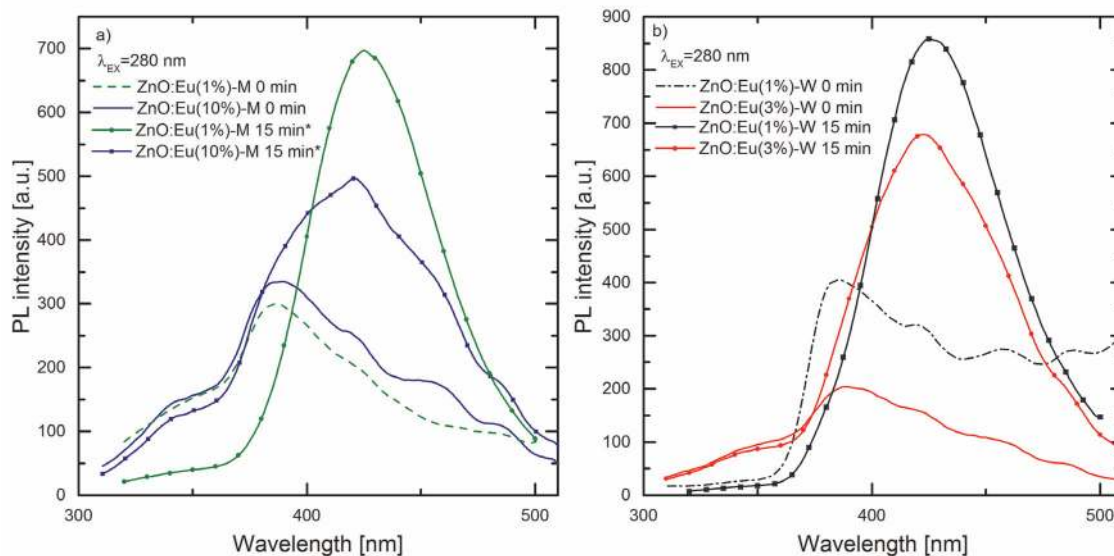
Fig. 10. Terephthalic acid PL emission at 0 min and after 15 min irradiation; with (*) are marked spectra done with PL filter to reduce emission peaks due to too strong emissions going out of range of measurable values in our apparatus

.

and 5%)-M samples, after 15 min irradiation, were recorded with filters in order to reduce emission peaks and put them to measuring levels of our device.
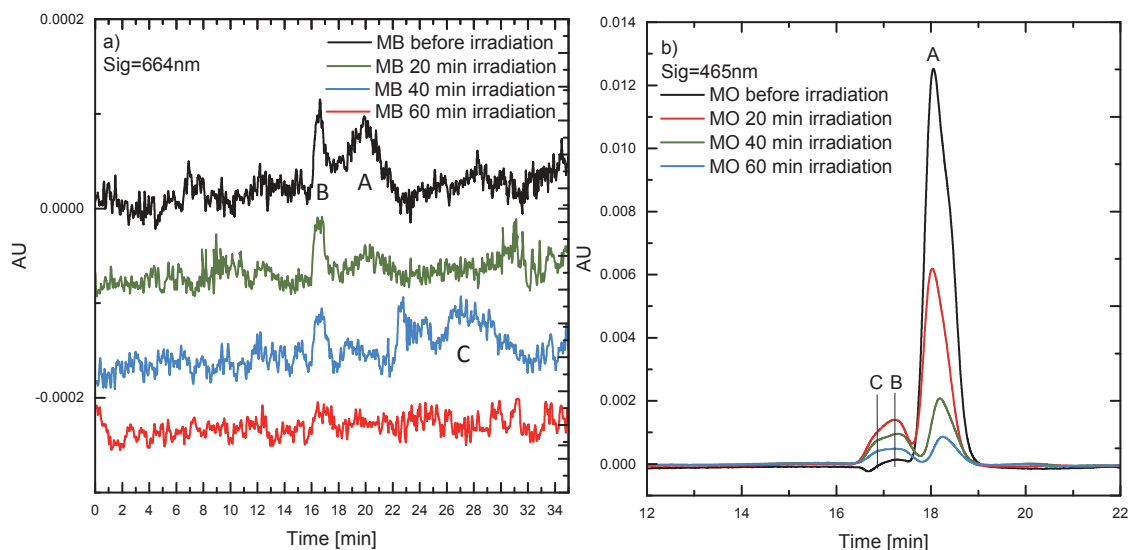

Fig. 11. HPLC analyses of (a) MB with initial solution at 15 ppm and (b) MO with initial solution at 15 ppm, after irradiation for 20, 40 and 60 min

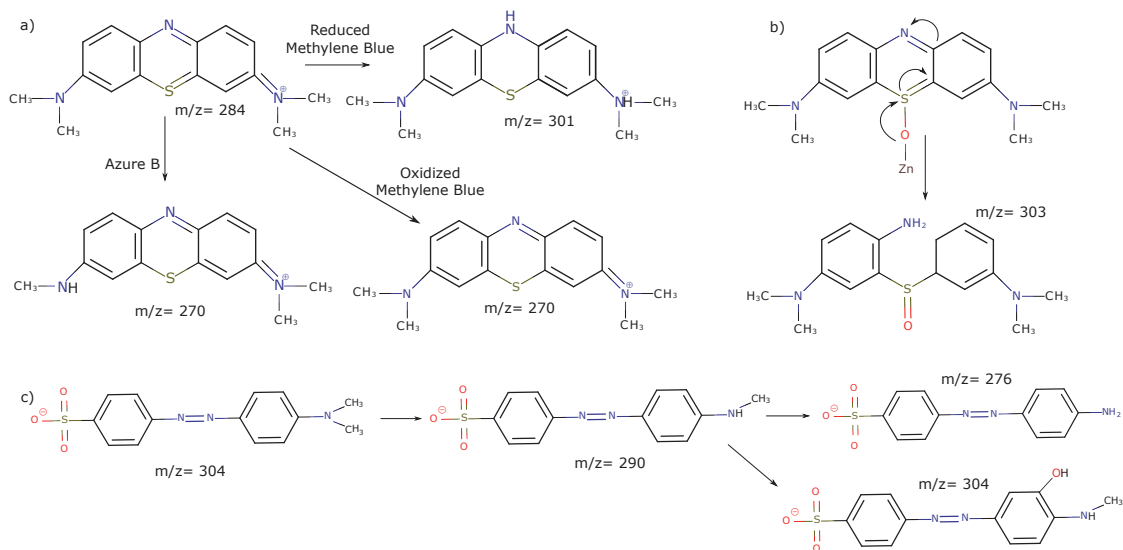In order to test the influence of various active species as well as leading importance of $^{\bullet}$OH radicals in

Fig. 12. Possible a) MB degradation path in the presence of •OH scavenger b) MB degradation path in the presence of hole scavenger c) MO degradation path in the presence of hole scavenger.

photocatalytic dye degradation we used hydroxyl (acetonitrile CH_3CN [92]) and hole (KI [93]) scavengers. To test holes by eliminating •OH radicals, MB was solved in acetonitrile (•OH scavenger) and ZnO:Eu(1%)-M and ZnO:Eu(1%)-W samples were added prior to the visible light irradiation. A fast decolorization was detected: solution with ZnO:Eu(1%)-M became completely colourless within 15 min and ZnO:Eu(1%)-W in 60 min. To examine such fast decolorization we added water (oxygen source), after which characteristic blue color of MB was returned, proving the existence of the colorless reduced form of MB, created from the reaction with holes (Figrure 12a) [94]. A reduced form of MB has intact chromophore groups meaning that •OH radicals are indeed needed for ring opening and complete degradation of dye. In next test we added KI (hole scavenger) to the solution of MB and acetonitril, previously mentioned, eliminating the holes together with the •OH radicals from the system and as expected, photocatalysis completely stopped. Further, effect of •OH radicals in photocatalysis were tested in the system where holes were eliminated: KI was added in to aqueous solution of MB. After illumination with visible light, purple colour was detected due to the purple Azure B (Figure 12b) creation [95, 96]. It seems that for MB photodegradation both hole and •OH radicals are important. When MB, as a cationic dye, is adsorbed or is near to the ZnO:Eu surface, •OH radical interact CS+ =C functional group. To conserve double bond conjugation, which is lost through the transformation from CS+ =C to CS(=O)C, central aromatic ring, containing S and N atoms, is opened as presented in Figure 12b. Hole induced H^+ (equation 6b) play an important role in the formation of CH and NH bonds [1, 97]. In the case of MO, when ZnO:Eu(1%)-M samples were added to MO dissolved in acetonitrile, photocatalytical efficiency was the same. However, when a hole scavenger (KI) was added to the

previously mention system, there was change in MO absorption spectrum, consisted of characteristic peak at 420 nm and much smaller at 368 nm. After 15 min irradiation, peak at 368 nm became dominant while peak at 420 nm lost its intensity. With prolonged irradiation only intensity of 368 nm peak increased. Possible explanations are: a) shift in the absorption band of MO directly related to molecular weight change [34]; b) interaction of MO with cationic parts [98, 99]. According to Chen et al. [34] the change in MO molecular weight by demethylation - substitution of the MO methyl group by the hydrogen atom (Figure 12c), can be the reason for the shift towards smaller wavelengths. In addition, as was reported previously, during the photocatalytic process demethylation is important in MO degradation [100]. However, hydroxylation of MO, in which the hydroxyl group connects to the ring of a chromophore is probably a part of MO degradation [101]. It should be taken into the account that the excessive concentration of anions on the nanoparticles surface can be a negative factor in the degradation of MO due to the competition of anions and MO for adsorption sites.

The HPLC chromatograms of 15 ppm MB degraded by ZnO:Eu(1%)-M under simulated sunlight for 20, 40 and 60 min, recorded at 664 nm are shown in Figure 11a. Peak A, at 19.84 min, represents the MB (m/z=284) while the peak at 16.56 min (peak B) is the self-degradation intermediate metabolite of MB [102]. After 20 min irradiation MB (peak A) degraded. While peak B is probably related to the MB where one methyl group left (m/z=270). This means that N-C bond between the methyl group and nitrogen atom is easy to be cleaved. After 40 min of irradiation we detected peak C at t_R=27.3 min that can be connected to the MB with the opened central ring (m/z=303) as presented in Figure 12b [1, 102]. In Figure 11b the HPLC profiles of MO (15 ppm) recorded at 465 nm and degraded at 0, 20, 40 and 60 min are presented. Peak A at t_R=18.05 min corresponds to MO (m/z=304). After 20 min of irradiation, besides lowering the intensity of peak A, consistent with MO degradation, peaks B and C appears at 17.23 min and 16.86 min, respectively. The appearance of peaks B and C can be from MO losing one (B (m/z=290)) or two methyl groups (C (m/z=276)) [103] which is in agreement with aforementioned results. But after 40 min of irradiation, beside all peaks loosing intensity, peak A shifts toward higher t_R=18.28 min, which might be explained by hydroxylation of once demethylated MO (m/z=306) [100]. Decreasing, without formation of new derivatives, with prolonged irradiation time, is suggesting that the transformation, as well as the chromophore breaking could proceed simultaneously. However, detailed analysis is needed to confirm our results.

4. Conclusions

The ZnO:Eu nanoparticles, synthesized with simple, fast and low-cost method, were confirmed and characterized by XRD, TEM, UV-vis, XPS and PL measurements. The photocatalytic activity, size of nanoparticles and ISP were influenced by Eu^{3+} doping and solvents. Size of the nanopraticles increased

for ZnO:Eu(1%)-W samples and decreased for ZnO:Eu(1%)-M samples with larger amount of Eu^{3+} ions. Decolorization and degradation of methylene blue and methyl orange was detected. In degradation of MB the most effective samples were ZnO:Eu(1%)-W and ZnO:Eu(1%)-M, while ZnO:Eu(3%)-W and ZnO:Eu(10%)-M were the most efficient in the case of MO. The improve charge separation of ZnO:Eu(x%)-M samples synthesized in methanol is considered the main reason for enhancement of dye photocatalytic degradation. Although $^{\bullet}$OH has been usually recognized as the most important active species of the photocatalytic degradation, our results showed that for degradation of MB combination of hole and hydroxyl radical formation is crucial, while for MO the formation of holes proved to be the most important factor.

References

[1] A. Houas, H. Lachheb, M. Ksibi, E. Elaloui, C. Guillard, J.-M. Herrmann, Photocatalytic degradation pathway of methylene blue in water, Appl. Catal., B. 31 (2001) 145–157.

[2] P. Pichat, Photocatalysis and water purification: From fundamentals to recent applications, John Wiley & Sons, 2013.

[3] J.-C. Sin, S.-M. Lam, I. Satoshi, K.-T. Lee, A. R. Mohamed, Sunlight photocatalytic activity enhancement and mechanism of novel europium-doped ZnO hierarchical micro/nanospheres for degradation of phenol, Appl. Catal., B. 148149 (2014) 258–268.

[4] M. Ahmad, E. Ahmed, Y. Zhang, N. R. Khalid, J. Xu, M. Ullah, Z. Hong, Preparation of highly efficient Al-doped ZnO photocatalyst by combustion synthesis, Curr. Appl Phys. 13 (4) (2013) 697–704.

[5] L. Andronic, A. Enesca, C. Vladuta, A. Duta, Photocatalytic activity of cadmium doped TiO2 films for photocatalytic degradation of dyes, Chem. Eng. J. 152 (1) (2009) 64–71.

[6] B. H. J. Bielski, D. E. Cabelli, R. L. Arudi, A. B. Ross, Reactivity of HO$_2$/O^{-2} radicals in aqueous solution, J. Phys. Chem. Ref. Data 14 (4) (1985) 1041–1100.

[7] X. Chang, J. Huang, Q. Tan, M. Wang, G. Ji, S. Deng, G. Yu, Photocatalytic degradation of PCP-Na over BiOI nanosheets under simulated sunlight irradiation, Catal. Commun. 10 (15) (2009) 1957–1961.

[8] C. Di Valentin, A. Selloni, Bulk and surface polarons in photoexcited anatase TiO$_2$, J. Phys. Chem. Lett. 2 (17) (2011) 2223–2228.

[9] S. Kuriakose, B. Satpati, S. Mohapatra, Enhanced photocatalytic activity of Co doped ZnO nanodisks and nanorods prepared by a facile wet chemical method, Phys. Chem. Chem. Phys. 16 (25) (2014) 12741–12749.

[10] S.-M. Lam, J.-C. Sin, A. Z. Abdullah, A. R. Mohamed, Transition metal oxide loaded ZnO nanorods: Preparation, characterization and their UVvis photocatalytic activities, Sep. Purif. Technol. 132 (2014) 378–387.

[11] C. Minero, G. Mariella, V. Maurino, E. Pelizzetti, Photocatalytic transformation of organic compounds in the presence of inorganic anions. 1. Hydroxyl-mediated and direct electron-transfer reactions of phenol on a titanium dioxidefluoride system, Langmuir 16 (6) (2000) 2632–2641.

[12] C. G. da Silva, J. L. Faria, Photochemical and photocatalytic degradation of an azo dye in aqueous solution by UV irradiation, J. Photoch. Photobio. A (2003) 133–143.

[13] C. S. Turchi, D. F. Ollis, Photocatalytic degradation of organic water contaminants: mechanisms involving hydroxyl radical attack, J. Catal. 122 (1990) 178–192.

[14] L. V. Trandafilović, R. K. Whiffen, S. Dimitrijević-Branković, M. Stoiljković, A. S. Luyt, V. Djoković, ZnO/Ag hybrid nanocubes in alginate biopolymer: Synthesis and properties, Chem. Eng. J. 253 (2014) 341–349.

[15] Z.-J. Jiang, C.-Y. Liu, L.-W. Sun, Catalytic properties of silver nanoparticles supported on silica spheres, J. Phys. Chem. B 109 (5) (2005) 1730–1735.

[16] R. L. Mayer, Compounds of quinone structure as allergens and cancerogenic agents, Experientia 6 (7) (1950) 241–250.

[17] L. Pereira, M. Alves, Dyes-Environmental Impact and Remediation, in: A. Malik, E. Grohmann (Eds.), Environmental Protection Strategies for Sustainable Development, Strategies for Sustainability, Springer Netherlands, 2012, pp. 111–162.

[18] H. Langhals, Color chemistry. Synthesis, properties and applications of organic dyes and pigments. 3rd revised edition. By Heinrich Zollinger., Angew. Chem. Int. Ed. 43 (40) (2004) 5291–5292.

[19] N. K. Singh, S. Saha, A. Pal, Methyl red degradation under UV illumination and catalytic action of commercial ZnO: a parametric study, Desalin. Water. Treat. 56 (2014) 1–11.

[20] J. Yu, X. Yu, Hydrothermal synthesis and photocatalytic activity of zinc oxide hollow spheres, Environ. Sci. Technol. 42 (13) (2008) 4902–4907.

[21] Y. Shiraishi, N. Saito, T. Hirai, Adsorption-driven photocatalytic activity of mesoporous titanium dioxide, J. Am. Chem. Soc. 127 (37) (2005) 12820–12822.

[22] S. Ardo, D. Achey, A. J. Morris, M. Abrahamsson, G. J. Meyer, Non-nernstian two-electron transfer photocatalysis at metalloporphyrin - TiO_2 interfaces, J. Am. Chem. Soc. 133 (41) (2011) 16572–16580.

[23] R. Enriquez, A. G. Agrios, P. Pichat, Probing multiple effects of TiO_2 sintering temperature on photocatalytic activity in water by use of a series of organic pollutant molecules, Catal. Today 120 (2) (2007) 196–202.

[24] T.-T. Chen, I.-C. Chang, M.-H. Yang, H.-T. Chiu, C.-Y. Lee, The exceptional photo-catalytic activity of ZnO/RGO composite via metal and oxygen vacancies, Appl. Catal., B. 142143 (2013) 442–449.

[25] F. Kayaci, C. Ozgit-Akgun, N. Biyikli, T. Uyar, Surface-decorated ZnO nanoparticles and ZnO nanocoating on electrospun polymeric nanofibers by atomic layer deposition for flexible photocatalytic nanofibrous membranes, RSC Adv. 3 (19) (2013) 6817–6820.

[26] W. Y. Teoh, J. A. Scott, R. Amal, Progress in heterogeneous photocatalysis: From classical radical chemistry to engineering nanomaterials and solar reactors, J. Phys. Chem. Lett. 3 (5) (2012) 629–639.

[27] L. Armelao, G. Bottaro, M. Pascolini, M. Sessolo, E. Tondello, M. Bettinelli, A. Speghini, Structureluminescence correlations in Europium-doped sol-gel ZnO nanopowders, J. Phys. Chem. C 112 (11) (2008) 4049–4054.

[28] M. Wang, C. Huang, Z. Huang, W. Guo, J. Huang, H. He, H. Wang, Y. Cao, Q. Liu, J. Liang, Synthesis and photoluminescence of Eu-doped ZnO microrods prepared by hydrothermal method, Opt. Mater. 31 (10) (2009) 1502–1505.

[29] M. Fu, Y. Li, S. wu, P. Lu, J. Liu, F. Dong, Solgel preparation and enhanced photocatalytic performance of Cu-doped ZnO nanoparticles, Appl. Surf. Sci. 258 (4) (2011) 1587–1591.

[30] E. Burunkaya, O. Kesmez, N. Kiraz, H. E. Çamurlu, M. Asiltürk, E. Arpaç, Sn^{4+} or Ce^{3+} doped TiO_2 photocatalytic nanometric films on antireflective nano-SiO_2 coated glass, Mater. Chem. Phys. 120 (23) (2010) 272–276.

[31] Y. Xie, C. Yuan, Characterization and photocatalysis of Eu^{3+}-TiO_2 sol in the hydrosol reaction system, Mater. Res. Bull. 39 (45) (2004) 533–543.

[32] P. Yang, C. Lu, N. Hua, Y. Du, Titanium dioxide nanoparticles co-doped with Fe^{3+} and Eu^{3+} ions for photocatalysis, Mater. Lett. 57 (4) (2002) 794–801.

[33] J. B. Zhong, J. Z. Li, X. Y. He, J. Zeng, Y. Lu, W. Hu, K. Lin, Improved photocatalytic performance of Pd-doped ZnO, Curr. Appl Phys. 12 (3) (2012) 998–1001.

[34] T. Chen, Y. Zheng, J.-M. Lin, G. Chen, Study on the photocatalytic degradation of methyl orange in water using Ag/ZnO as catalyst by liquid chromatography electrospray ionization ion-trap mass spectrometry, J. Am. Soc. Mass Spectrom. 19 (7) (2008) 997–1003.

[35] L. F. M. Ismail, M. M. Emara, M. M. El-Moselhy, N. A. Maziad, O. K. Hussein, Silica coating and photocatalytic activities of ZnO nanoparticles: Effect of operational parameters and kinetic study, Spectrochim. Acta, Part A 131 (2014) 158–168.

[36] M. M. Khan, J. Lee, M. H. Cho, Au@TiO_2 nanocomposites for the catalytic degradation of methyl orange and methylene blue: An electron relay effect, J. Ind. Eng. Chem. 20 (4) (2014) 1584–1590.

[37] S. J. Pearton, D. P. Norton, K. Ip, Y. W. Heo, T. Steiner, Recent progress in processing and properties of ZnO, Prog. Mater Sci. 50 (3) (2005) 293–340.

[38] M. Miyauchi, A. Nakajima, T. Watanabe, K. Hashimoto, Photocatalysis and photoinduced hydrophilicity of various metal oxide thin films, Chem. Mater. 14 (6) (2002) 2812–2816.

[39] L. Armelao, D. Barreca, G. Bottaro, A. Gasparotto, D. Leonarduzzi, C. Maragno, E. Tondello, C. Sada, Tailored synthesis of ZnO:Er(III) nanosystems by a hybrid rf-sputtering/sol-gel route, J. Vac. Sci. Technol., A 24 (5) (2006) 1941–1947.

[40] C. Karunakaran, P. Gomathisankar, G. Manikandan, Preparation and characterization of antimicrobial Ce-doped ZnO nanoparticles for photocatalytic detoxification of cyanide, Mater. Chem. Phys. 123 (23) (2010) 585–594.

[41] M. Khatamian, A. A. Khandar, B. Divband, M. Haghighi, S. Ebrahimiasl, Heterogeneous photocatalytic degradation of 4-nitrophenol in aqueous suspension by Ln (La^{3+}, Nd^{3+} or Sm^{3+}) doped ZnO nanoparticles, J. Mol. Catal. A: Chem. 365 (2012) 120–127.

[42] M. Wang, C. Huang, Z. Huang, W. Guo, J. Huang, H. He, H. Wang, Y. Cao, Q. Liu, J. Liang, Synthesis and photoluminescence of Eu-doped ZnO microrods prepared by hydrothermal method, Cryst. Eng. Comm 31 (10) (2014) 1502–1505.

[43] D. Daksh, Y. K. Agrawal, Rare earth-doped zinc oxide nanostructures: A review, Rev. Nanosci. Nanotechnol. 5 (2016) 1–27.

[44] J.-C. Sin, S.-M. Lam, Hydrothermal synthesis of europium-doped flower-like ZnO hierarchical structures with enhanced sunlight photocatalytic degradation of phenol, Mater. Lett. 182 (2016) 223–226.

[45] P. V. Korake, A. N. Kadam, K. M. Garadkar, Photocatalytic activity of Eu^{3+}-doped ZnO nanorods synthesized via microwave assisted technique, J. Rare Earths 32 (4) (2014) 306–313.

[46] Y. Zong, Z. Li, X. Wang, J. Ma, Y. Men, Synthesis and high photocatalytic activity of Eu-doped ZnO nanoparticles, Ceram. Int. 40 (7, Part B) (2014) 10375–10382.

[47] A. Phuruangrat, O. Yayapao, T. Thongtem, S. Thongtem, Synthesis and characterization of Europium-doped zinc oxide photocatalyst, J. Nanomater. 2014 (2014) e367529.

[48] K. Kobayakawa, Y. Nakazawa, M. Ikeda, Y. Sato, A. Fujishima, Influence of the density of surface hydroxyl groups on TiO_2 photocatalytic activities, Ber. Bunsenges. Phys. Chem. 94 (12) (1990) 1439–1443.

[49] H. Lin, J. Long, Q. Gu, W. Zhang, R. Ruan, Z. Li, X. Wang, In situ IR study of surface hydroxyl species of dehydrated TiO2: towards understanding pivotal surface processes of TiO_2 photocatalytic oxidation of toluen, Phys. Chem. Chem. Phys. 14 (26) (2012) 9468–9474.

[50] T. L. Thompson, J. T. Yates, Monitoring hole trapping in photoexcited TiO_2 (110) using a surface photoreaction, J. Phys. Chem. B 109 (39) (2005) 18230–18236.

[51] O. Micic, Y. Zhang, K. R. Cromack, A. D. Trifunac, M. C. Thurnauer, Photoinduced hole transfer from titanium dioxide to

methanol molecules in aqueous solution studied by electron paramagnetic resonance, J. Phys. Chem. 97 (1993) 13284–13288.

[52] W. Hirschwald, D. Hofmann, Interaction of methanol with ZnO surfaces at low temperatures, Surf. Sci. 140 (2) (1984) 415–424.

[53] A. B. Sherrill, M. A. Barteau, Chapter 10 - Principles of Reactivity from Studies of Organic Reactions on Model Oxide Surfaces, in: D. P. Woodruff (Ed.), The Chemical Physics of Solid Surfaces, Vol. 9 of Oxide Surfaces, Elsevier, 2001, pp. 409–442.

[54] E. Brillas, J. Casado, Aniline degradation by Electro-Fenton® and peroxi-coagulation processes using a flow reactor for wastewater treatment, Chemosphere 47 (3) (2002) 241–248.

[55] H. Sawada, R. Wang, A. W. Sleight, An electron density residual study of zinc oxide, J. Solid State Chem. 122 (1) (1996) 148–150.

[56] J. Yang, X. Li, J. Lang, L. Yang, M. Wei, M. Gao, X. Liu, H. Zhai, R. Wang, Y. Liu, J. Cao, Synthesis and optical properties of Eu-doped ZnO nanosheets by hydrothermal method, Mater. Sci. Semicond. Process. 14 (34) (2011) 247–252.

[57] S. Mathur, S. S. Ray, Nanostructured Materials and Nanotechnology VI: Ceramic Engineering and Science Proceedings, Volume 33, John Wiley & Sons, 2012.

[58] F. Kayaci, S. Vempati, I. Donmez, N. Biyikli, T. Uyar, Role of zinc interstitials and oxygen vacancies of ZnO in photocatalysis: a bottom-up approach to control defect density, Nanoscale 6 (17) (2014) 10224–10234.

[59] L. Schmidt-Mende, J. L. MacManus-Driscoll, ZnO - nanostructures, defects, and devices, Mater. Today 10 (5) (2007) 40–48.

[60] K. Vanheusden, C. Seager, W. Warren, D. Tallant, J. Voigt, Correlation between photoluminescence and oxygen vacancies in ZnO phosphors, Appl. Phys. Lett. 68 (3) (1996) 403–405.

[61] Q. Yang, K. Tang, J. Zuo, Y. Qian, Synthesis and luminescent property of single-crystal ZnO nanobelts by a simple low temperature evaporation route, Appl. Phys. A 79 (8) (2004) 1847–1851.

[62] D. Zhang, Q. Wang, Z. Xue, Photoluminescence of ZnO films excited with light of different wavelength, Appl. Surf. Sci. 207 (1-4) (2003) 20–25.

[63] H. Zhou, H. Alves, D. M. Hofmann, W. Kriegseis, B. K. Meyer, G. Kaczmarczyk, A. Hoffmann, Behind the weak excitonic emission of ZnO quantum dots: ZnO/Zn(OH)$_2$ core-shell structure, Appl. Phys. Lett. 80 (2) (2002) 210–212.

[64] A. B. Djurišić, Y. H. Leung, K. H. Tam, Y. F. Hsu, L. Ding, W. K. Ge, Y. C. Zhong, K. S. Wong, W. K. Chan, H. L. Tam, K. W. Cheah, W. M. Kwok, D. L. Phillips, Defect emissions in ZnO nanostructures, Nanotechnology 18 (9) (2007) 095702.

[65] S. M. Ahmed, P. Szymanski, L. M. El-Nadi, M. A. El-Sayed, Energy-Transfer Efficiency in Eu-Doped ZnO Thin Films: The Effects of Oxidative Annealing on the Dynamics and the Intermediate Defect States, ACS Appl. Mater. Interfaces 6 (3) (2014) 1765–1772.

[66] C. Ronda (Ed.), Luminescence: From Theory to Applications, Wiley-VCH, Berlin, 2008.

[67] V. Kumar, V. Kumar, S. Som, M. M. Duvenhage, O. M. Ntwaeaborwa, H. C. Swart, Effect of Eu doping on the photoluminescence properties of ZnO nanophosphors for red emission applications, Appl. Surf. Sci. 308 (2014) 419–430.

[68] G. Socrates, Wiley: Infrared and Raman Characteristic Group Frequencies: Tables and Charts, 3rd Edition, John Wiley & Sons,LTD, 2002.

[69] D. L. Golić, Z. Branković, N. Daneu, S. Bernik, G. Branković, Solvothermal syntheses of nano- and micro-sized ZnO powders with a controllable morphology, J. Sol-Gel. Sci. Technol. 63 (1) (2012) 116–125.

[70] B. H. Stuart, Infrared Spectroscopy: Fundamentals and Applications, Wiley, 2004.

[71] M. F. Khan, A. H. Ansari, M. Hameedullah, E. Ahmad, F. M. Husain, Q. Zia, U. Baig, M. R. Zaheer, M. M. Alam, A. M. Khan, Z. A. Alothman, I. Ahmad, G. M. Ashraf, G. Aliev, Sol-gel synthesis of thorn-like ZnO nanoparticles endorsing mechanical stirring effect and their antimicrobial activities: Potential role as nano-antibiotics, Sci. Rep. 6 (2016) 27689.

[72] A. Prakash, S. K. Misra, D. Bahadur, The role of reduced graphene oxide capping on defect induced ferromagnetism of ZnO nanorods, Nanotechnology 24 (9) (2013) 095705.

[73] D. Briggs, Handbook of X-ray Photoelectron Spectroscopy, Surf. Interface Anal. 3 (1981) 195.

[74] D. Kumar, Y.-F. Han, M. S. Chen, D. W. Goodman, Kinetic and spectroscopic studies of vinyl acetate synthesis over Pd(100),

Catal. Lett. 106 (1-2) (2006) 1–5.

[75] R. Hunger, W. Jaegermann, A. Merson, Y. Shapira, C. Pettenkofer, J. Rappich, Electronic structure of methoxy-, bromo-, and nitrobenzene grafted onto Si(111), J. Phys. Chem. B 110 (31) (2006) 15432–15441.

[76] M. A. Henderson, A surface science perspective on TiO_2 photocatalysis, Surf. Sci. Rep. 66 (67) (2011) 185–297.

[77] F. Mercier, C. Alliot, L. Bion, N. Thromat, P. Toulhoat, XPS study of Eu(III) coordination compounds: Core levels binding energies in solid mixed-oxo-compounds EumXxOy, J. Electron Spectrosc. Relat. Phenom. 150 (1) (2006) 21–26.

[78] C. Rameshan, W. Stadlmayr, S. Penner, H. Lorenz, L. Mayr, M. Hvecker, R. Blume, T. Rocha, D. Teschner, A. Knop-Gericke, R. Schlgl, D. Zemlyanov, N. Memmel, B. Kltzer, In situ XPS study of methanol reforming on PdGa near-surface intermetallic phases, J. Catal. 290 (100) (2012) 126–137.

[79] G. K. Ramesha, A. Vijaya Kumara, H. B. Muralidhara, S. Sampath, Graphene and graphene oxide as effective adsorbents toward anionic and cationic dyes, J. Colloid Interface Sci. 361 (1) (2011) 270–277.

[80] M. A. Lazar, W. A. Daoud, Selective adsorption and photocatalysis of low-temperature base-modified anatase nanocrystals, RSC Adv. 2 (2) (2011) 447–452.

[81] M. Kosmulski, Chemical Properties of Material Surfaces, CRC Press, 2001.

[82] R. F. Domingos, Z. Rafiei, C. E. Monteiro, M. A. Khan, K. J. Wilkinson, Agglomeration and dissolution of zinc oxide nanoparticles: role of pH, ionic strength and fulvic acid, Environ. Chem. 10 (4) (2013) 306–312.

[83] F. Mohd Omar, H. Abdul Aziz, S. Stoll, Aggregation and disaggregation of ZnO nanoparticles: Influence of pH and adsorption of Suwannee River humic acid, Sci. Total Environ. 468–469 (2014) 195–201.

[84] A. Emeline, V. Ryabchuk, N. Serjone, Factors affecting the efficiency of a photocatalysed process in aqueous metal-oxide dispersions, prospect of distinguishing between two kinetic models, J. Photochem. Photobio. A 133 (2000) 89–97.

[85] Y. S. Ho, G. McKay, Pseudo-second order model for sorption processes, Process Biochem. 34 (5) (1999) 451–465.

[86] Y.-S. Ho, Review of second-order models for adsorption systems, J. Hazard. Mater. 136 (3) (2006) 681–689.

[87] K. A. Connors, Chemical Kinetics: The Study of Reaction Rates in Solution, John Wiley & Sons, 1990.

[88] Y. S. Ho, G. McKay, The kinetics of sorption of divalent metal ions onto sphagnum moss peat, Water Res. 34 (3) (2000) 735–742.

[89] Y. Zheng, C. Chen, Y. Zhan, X. Lin, Q. Zheng, K. Wei, J. Zhu, Y. Zhu, Luminescence and photocatalytic activity of ZnO nanocrystals: Correlation between structure and property, Inorg. Chem. 46 (16) (2007) 6675–6682.

[90] Z. Xiong, L. L. Zhang, J. Ma, X. S. Zhao, Photocatalytic degradation of dyes over graphene¢gold nanocomposites under visible light irradiation, Chem. Commun. 46 (33) (2010) 6099–6101.

[91] V. V. Shvalagin, A. L. Stroyuk, S. Y. Kuchmii, Photochemical synthesis of ZnO/Ag nanocomposites, J. Nanopart. Res. 9 (3) (2006) 427–440.

[92] S. Mitroka, S. Zimmeck, D. Troya, J. M. Tanko, How solvent modulates hydroxyl radical reactivity in hydrogen atom abstractions, J. Am. Chem. Soc. 132 (9) (2010) 2907–2913.

[93] Y. Wang, P. Zhang, Photocatalytic decomposition of perfluorooctanoic acid (PFOA) by TiO_2 in the presence of oxalic acid, J. Hazard. Mater. 192 (3) (2011) 1869–1875.

[94] S.-A. Ong, E. Toorisaka, M. Hirata, T. Hano, Biodegradation of redox dye Methylene Blue by up-flow anaerobic sludge blanket reactor, J. Hazard. Mater. 124 (1-3) (2005) 88–94.

[95] A. Katafias, M. Lipińska, K. Strutyński, Alkaline hydrogen peroxide as a degradation agent of methylene blue-kinetic and mechanistic studies, Reac. Kinet. Mech. Cat. 101 (2) (2010) 251–266.

[96] W. J. MacNeal, J. A. Killian, Chemical studies on polychrome methylene blue, J. Am. Chem. Soc. 48 (3) (1926) 740–747.

[97] M. J. Plater, A degradation product of methylene blue, ARKIVOC 2003 (1) (2003) 37–42.

[98] R. K. Dutta, S. N. Bhat, Interaction of methyl orange with submicellar cationic surfactants., Bull. Chem. Soc. Jpn. 66 (9) (1993) 2457–2460.

[99] K. K. Karukstis, D. A. Savin, C. T. Loftus, N. D. D'Angelo, Spectroscopic studies of the Interaction of methyl orange with cationic alkyltrimethylammonium bromide ssurfactants, J. Colloid Interface Sci. 203 (1) (1998) 157–163.

[100] C. Baiocchi, M. C. Brussino, E. Pramauro, A. B. Prevot, L. Palmisano, M. Giuseppe, Characterization of methyl orange and its photocatalytic degradation products by HPLC/UV-VIS diode array and atmospheric pressure ionization quadrupole ion trap mass spectrometry, Int. J. Mass Spectrom. 214 (2) (2002) 247–256.

[101] K. Dai, H. Chen, T. Peng, D. Ke, H. Yi, Photocatalytic degradation of methyl orange in aqueous suspension of mesoporous titania nanoparticles, Chemosphere 69 (9) (2007) 1361–1367.

[102] R. Zuo, G. Du, W. Zhang, L. Liu, Y. Liu, L. Mei, Z. Li, Photocatalytic degradation of methylene blue using TiO_2 impregnated diatomite, Advances in Materials Science and Engineering 2014 (2014) e170148.

[103] A. B. Prevot, A. Basso, C. Baiocchi, M. Pazzi, G. Marci, V. Augugliaro, L. Palmisano, E. Pramauro, Analytical control of photocatalytic treatments: degradation of a sulfonated azo dye, Anal. Bioanal. Chem. 378 (1) (2004) 214–220.